ISSN 1064-2269, Journal of Communications Technology and Electronics, 2022, Vol. 67, No. 4, pp. 430–442. © Pleiades Publishing, Inc., 2022.

THEORY AND METHODS OF SIGNAL PROCESSING

Weak Pulse Signal Detection Based on the Broad Learning Method under the Chaotic Background

L. Su[a], * and J. Yang[a]

[a] *School of Science, Chongqing University of Technology, Chongqing, 400054 Republic of China*

**e-mail: cloudhopping@163.com*

Received September 22, 2021; revised October 21, 2021; accepted December 7, 2021

Abstract—This paper combines the broad learning method with signal detection to realize weak pulse signal detection under the chaotic background. First, based on the short-term predictability and sensitivity to small perturbations of chaotic signals, the phase space reconstruction of the observed signals is carried out. Second, the robust manifold width adaptive detection (RMWAD) model is constructed to obtain the one-step prediction error, and then, we could realize adaptive detection of weak pulse signals by using one-step prediction error and hypothesis test. Finally, we evaluate detection performance by Receiver Operating Characteristic curve, precision rate, recall rate, accuracy rate and F1 score. Simulation experiments shows that the RMWAD model could effectively detect weak pulse signals under the chaotic background, and the model has better detection performance than the broad learning system (BLS), back propagation (BP) neural network model, Extreme Gradient Boosting (XGB) model and support vector regression (SVR) model.

Keywords: chaos, broad learning, weak pulse signal, detection

DOI: 10.1134/S1064226922040106

INTRODUCTION

Weak signals are extremely weak and difficult to be detected, and its detection technology has broad application prospects in radar, communication transmission, sea clutter processing and seismic detection [1–4]. The traditional weak signal detection methods mainly include stochastic resonance method [5, 6], lock-in amplifier method [7, 8] and Duffing oscillator method [9, 10], but these methods is basically invalid for weak signal detection under chaotic background, and has a high threshold for the signal-to-noise ratio (SNR) of weak signal detection. With the development of chaos theory, the method of combining chaos theory with weak signal does not need to consider the distribution characteristics of interference, and it also does not need a lot of prior knowledge to effectively achieve a lower SNR threshold [11–14]. In addition, the pulse signal is a typical signal in communication, seismic detection and fault diagnosis and other fields [15, 16], so effectively improving the detection ability of weak pulse signal under chaotic background is of great significance to reduce the detection cost of equipment and enhance the anti-interference ability of detection system.

Therefore, scholars from home and abroad have carried out extensive research on the detection of weak pulse signal under chaotic background. Some nonlinear methods such as least squares support vector machine, Elman neural network and so on are used to detect weak pulse signals under chaotic background [17–22], these methods have certain robustness and generalization ability, but the selection of the original data and factors has a great impact on the prediction results, and fail to use the chaotic nature, resulting in the low reliability of the prediction [12, 23]. Is there any other way? Broad learning system is a neural network structure independent of depth structure. Compared with "depth" structure, "width" structure is very concise because there is no coupling between layers [24]. Based on the broad learning method, a structured manifold width learning system improved the fitting effect of large-scale chaotic data [25]. Besides, a robust manifold broad learning system further improved the generalization ability and robustness of the model, and demonstrated that the model is superior to other broad learning models for chaotic data prediction [26]. In addition, the fusion model based on principal component analysis and broad learning algorithm is feasible in the fault diagnosis of rotor system [27]. In practice, since the broad learning method was proposed, it has been widely used in image classification, pattern recognition, EEG signal processing and other fields, it's a promising machine learning algorithm [28–33].

According to the broad learning method could better describe the properties of nonlinear characteristics,

and in order to realize intelligence statistical detection, this paper proposed the robust manifold width adaptive detection (RMWAD) model, which is applied to obtain one-step prediction error, hypothesis testing is used to realize weak pulse signal detection under chaotic noise background.

The remainder of the paper is organized as follows. In Section 1, we provide the background for broad learning system and hypothesis test of weak pulse signal. In Section 2, we present the detection model. In Section 3, we illustrate the simulation experiments of the detection model. We summarize the results of simulation experiments in Conclusion section.

1. DESCRIPTION OF CONCEPTS

1.1. Broad Learning System

Broad learning system (BLS) based on random vector function connection network (RALFNN) is a neural network, the mainly difference is that BLS model extracts the features from original data and take the features as the input layer compared with RALFNN [24, 34]. Supposing there are n kinds of mapping methods, and each method has q nodes, we consider the mapped feature

$$\mathbf{Z} = \varphi(\mathbf{SW} + \boldsymbol{\beta}), \tag{1}$$

where $\varphi(.)$ is activation function, $\mathbf{S} \in \mathbf{R}^{r\times m}$ is the input data, r is the number of samples, m is the dimension of samples, $\mathbf{Z} = \{\mathbf{Z}_i, i = 1,2,\ldots,n\}$, $\mathbf{W} = \{\mathbf{W}_i, i = 1,2,\ldots,n\}$, $\mathbf{W}_i \in \mathbf{R}^{m\times q}$ is the weight of mapping features, $\boldsymbol{\beta} = \{\boldsymbol{\beta}_i, i = 1,2,\ldots,n\}$ is bias.

The following are similar with RALFNN. Supposing there are p enhancement nodes, then we could receive enhanced information

$$\mathbf{H} = \zeta(\mathbf{ZW}_{\text{up}} + \boldsymbol{\beta}_{\text{up}}), \tag{2}$$

where $\mathbf{H} = \{\mathbf{H}_j, j = 1,2,\ldots,p\}$, $\mathbf{W}_{\text{up}}, \boldsymbol{\beta}_{\text{up}}$ are generated randomly, and $\zeta(.)$ is activation function.

We could receive the output of BLS model

$$\mathbf{Y} = [\mathbf{Z}|\mathbf{H}]\mathbf{W}_{\text{out}}, \tag{3}$$

where $\mathbf{W}_{\text{out}}$ are obtained by ridge regression algorithm [35].

Based on the BLS model, many other great new models are proposed, such as fuzzy broad learning model, structured manifold broad learning model and robust manifold broad learning model, these models have achieved satisfactory performance on chaotic time series, especially robust manifold broad learning model has great robustness and generalization ability, and is superior to other broad learning methods for chaotic time series prediction [24–26, 36].

1.2. Hypothesis Test of Weak Pulse Signal

The weak pulse signal could be transformed in the chaotic background noise

$$\begin{aligned} H_0 &: s(t) = n(t) + e(t), \\ H_1 &: s(t) = n(t) + u(t) + e(t), \end{aligned} \tag{4}$$

where $s(t)$ represents the observation signal, $n(t)$ represents the chaotic signal, $u(t)$ represents the weak pulse signal, $e(t)$ represents Gaussian white noise.

The weak pulse signal is often submerged in the chaotic noise, if the hypothesis test is directly inferred by equation (4), it's prone to high false positive [17]. But we could obtain the estimation of the chaotic noise based on its chaotic nonlinear characteristics, and then the hypothesis testing problem is further transformed

$$\begin{aligned} H_0 &: s(t) - n(t) = e(t), \\ H_1 &: s(t) - n(t) = u(t) + e(t), \end{aligned} \tag{5}$$

when H_0 is true, it shows that there is only white Gaussian noise in the observed signal, and there is no weak pulse signal; when the H_1 is true, it shows that there is a weak pulse signal in the observation signal.

In this paper, we consider construct a robust manifold width dynamic adaptive detection (RMWAD) model based on broad learning methods to detect the weak pulse signal from prediction error. The specific idea framework of this paper is shown in Fig. 1.

2. DETECTION MODEL

2.1. RMWAD Model

According to the Section 1, we need to obtain the estimation of the chaotic noise, then the prediction error could be computed, and the hypothesis test (5) is used to detect the weak pulse signal, so the detection model RMWAD is mainly divided into the following three steps: first, reconstructing the one dimensional observation signal into a high dimensional matrix; then, establishing the RMWAD model to obtain the one-step prediction error; finally, detecting weak pulse signal from prediction error by the hypothesis testing.

2.2. Reconstruction Observation Signal

Phase space is used to represent all possible states of a system. The dimension of nonlinear system is usually relatively high, but the time series collected in practice are generally one-dimensional and difficult to reflect the high-dimensional space of nonlinear system [37, 38]. So we need to extend the collected time series to a higher dimensional phase space. For the

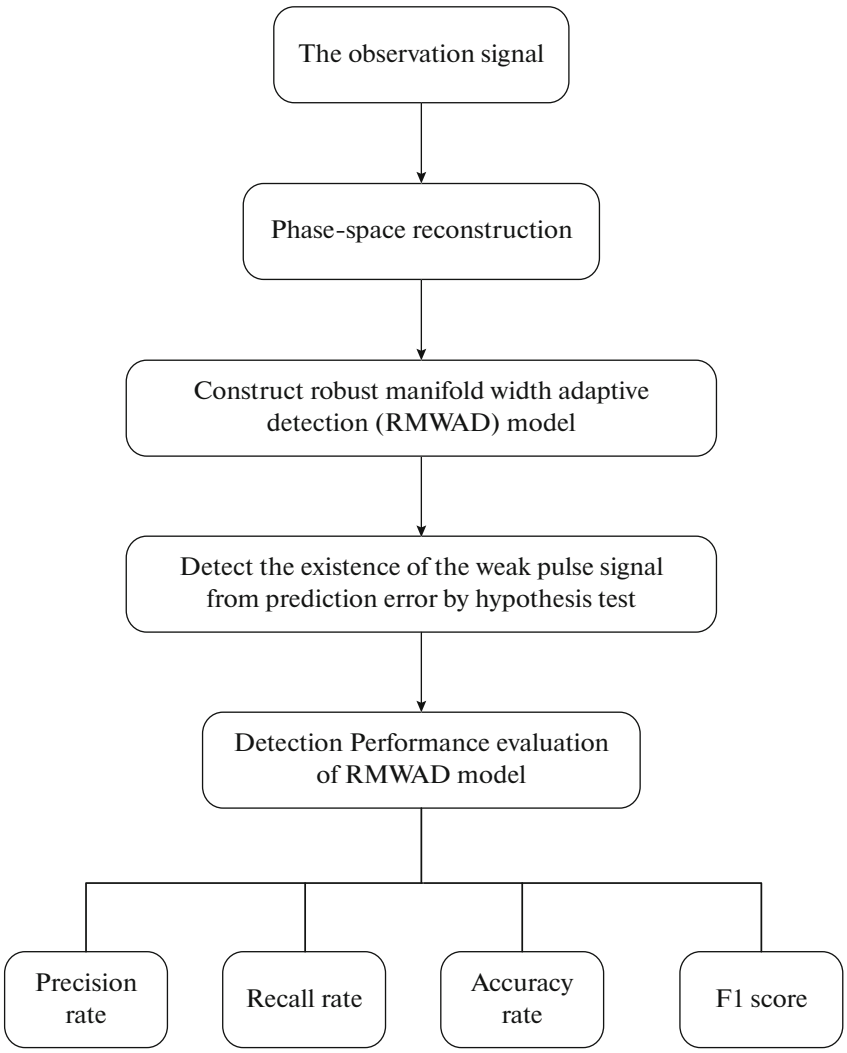

Fig. 1. The specific idea framework of weak pulse signal detection.

observation signal $\{s(t), t = 1,2,\ldots,n\}$, we could receive its phase in high-dimensional space

$$\mathbf{S}(t) = (s(t), s(t-\tau), \ldots, s(t-(m-1)\tau)), \qquad (6)$$

where $t = n_1, n_1+1, \ldots, n$; $n_1 = 1+(m-1)\tau$; m is embedding dimension obtained by the method proposed by Cao [39], τ is the delay time obtained by the auto-correlation method [40].

According to Takens' theorem [37], If we could find a smooth mapping h: $\mathbf{R}^m \to \mathbf{R}$ or an estimation $\hat{h}$ of h, then the data of the next time could be predicted, that is $s(t+1) = h(\mathbf{S}(t))$ or $s(t+1) \approx \hat{h}(\mathbf{S}(t))$. Therefore, we could construct the RMWAD model [24–26] as the approximate mapping $\hat{h}$ to receive one-step prediction.

2.3. RMWAD Model

For the reconstructed observation signal $\mathbf{S}(t)$, supposing that the feature layer of the RMWAD model has n kinds of mapping methods, each method has q nodes, and then we could receive the mapped feature (1).

Because the time series in chaotic dynamic system usually evolve according to a certain manifold, it is necessary to represent the reconstructed observation signal by manifold [41], and we could express the objective function of manifold feature mapping.

$$\begin{gathered}\min \operatorname{tr}\left((\mathbf{SW})^T \mathbf{D}(\mathbf{SW})\right) + \alpha\|\mathbf{SW}-\mathbf{B}\|_F^2 + \gamma\|\mathbf{W}\|_{2,1}, \\ \text{s.t.}(\mathbf{SW})^T \mathbf{G}(\mathbf{SW}) = \mathbf{I},\end{gathered} \qquad (7)$$

where tr denotes the operation of finding the trace of a matrix; $\mathbf{W}$ is the weight in the feature layer; α and γ are regularization parameters; $\mathbf{B} \in \mathbf{R}^{r\times q}$ is randomly

generated perturbation matrix; r is the number of rows of $\mathbf{S}$; q is the number of the mapping feature; $\mathbf{D} = \mathbf{G}^{-1/2}(\mathbf{G}-\mathbf{Q})\mathbf{G}^{-1/2}$ is the normalized graph Laplacian matrix; s.t. stands for the phrase of "subject to"; $\mathbf{I}$ is the unit matrix; ^{T} denotes the operation of transpose; $\mathbf{G}$ is the diagonal matrix denoted as $G_{ii} = \sum_i Q_{ij}$, where

$$Q_{ij} = \begin{cases} \exp\left(-\dfrac{\|\mathbf{s}_i - \mathbf{s}_j\|^2}{\sigma^2}\right), & \mathbf{s}_i \in N_k(\mathbf{s}_j),\ \mathbf{s}_j \in N_k(\mathbf{s}_i), \\ 0, & \text{otherwise}, \end{cases} \tag{8}$$

where $N_k(\mathbf{S})$ represents the k nearest neighbor sets of $\mathbf{S}$.

$\mathbf{S}$ is reconstructed observation signal, $\mathbf{D}$ and $\mathbf{G}$ could be obtained by $\mathbf{S}$ and Q_{ij}. But the objective function (7) is the non-convex and non-smooth function with generalized orthogonal constraints and it's difficult to be optimized. Therefore, we need the following methods to optimize the objective function (7):

First, we use separating variables method [42] to obtain the new objective function

$$\begin{aligned} &\min \operatorname{tr}\left((\mathbf{SW})^T \mathbf{D}(\mathbf{SW})\right) \\ &+ \alpha\|\mathbf{SW}-\mathbf{B}\|_F^2 + \gamma\|\mathbf{R}\|_{2,1} + \xi(\mathbf{H}), \\ &\text{s.t. } \mathbf{H} - \mathbf{G}^{1/2}\mathbf{SW} = 0, \quad \mathbf{R} - \mathbf{W} = 0, \end{aligned} \tag{9}$$

where $\xi(\mathbf{H}) = \begin{cases} 0, & \mathbf{H}^T\mathbf{H} = \mathbf{I}, \\ \infty, & \text{otherwise}, \end{cases}$

and

$$\|\mathbf{R}\|_{2,1} = \sum_{i=1}^{m}\sqrt{\sum_{i=1}^{q} R_{ij}^2}. \tag{10}$$

Second, we could receive the augmented Lagrange function of the objective function (9)

$$\begin{aligned} &\mathbf{L}(\mathbf{W},\mathbf{R},\mathbf{H},\boldsymbol{\lambda}1,\boldsymbol{\lambda}2;\rho) \\ &= \operatorname{tr}\left(\mathbf{W}^T\mathbf{S}^T\mathbf{DSW}\right) + \alpha\|\mathbf{SW}-\mathbf{B}\|_F^2 \\ &+ \gamma\|\mathbf{R}\|_{2,1} + \xi(\mathbf{H}) + \frac{\rho}{2}\left\|\mathbf{R}-\mathbf{W}+\frac{\boldsymbol{\lambda}1}{\rho}\right\|_F^2 \\ &+ \frac{\rho}{2}\left\|\mathbf{H}-\mathbf{G}^{1/2}\mathbf{SW}+\frac{\boldsymbol{\lambda}2}{\rho}\right\|_F^2. \end{aligned} \tag{11}$$

Third, according to the augmented Lagrange function (11), the iterative equations [26, 43, 44] are as follows

$$\begin{cases} \mathbf{W}_k = (\mathbf{part})^{-1}\left(\left(2\alpha\mathbf{S}^T\mathbf{B} + \rho\left(\mathbf{R}_k + \dfrac{\boldsymbol{\lambda}1_k}{\rho}\right)\right) + \rho\mathbf{S}^T\mathbf{G}^{T/2}\left(\mathbf{H}_k + \dfrac{\boldsymbol{\lambda}2_k}{\rho}\right)\right), \quad \rho > 0, \\ \mathbf{R}_{k+1} = \dfrac{\max\{\|\mathbf{v}\|_2 - \tau, 0\}}{\max\{\|\mathbf{v}\|_2 - \tau, 0\} + \tau}\left(\mathbf{W}_k - \dfrac{\boldsymbol{\lambda}1_k}{\rho}\right), \quad \tau = \dfrac{\gamma}{\rho}, \\ \mathbf{H}_{k+1} = \left(\mathbf{I} + \dfrac{\rho}{2}\mathbf{L}\right)^{-1}\left(\mathbf{I} - \dfrac{\rho}{2}\mathbf{L}\right)\mathbf{H}_k, \\ \boldsymbol{\lambda}1_{k+1} = \boldsymbol{\lambda}1_k + \rho(\mathbf{R}_k - \mathbf{W}_k), \\ \boldsymbol{\lambda}2_{k+1} = \boldsymbol{\lambda}2_k + \rho\left(\mathbf{H}_k - \mathbf{G}^{1/2}\mathbf{SW}_k\right), \end{cases} \tag{12}$$

where $\mathbf{part} = 2\mathbf{S}^T\mathbf{DS} + 2\alpha\mathbf{S}^T\mathbf{S} + \rho\mathbf{I} + \rho\mathbf{S}^T\mathbf{GS}$, $\mathbf{R}_k \in \mathbf{R}^{m\times q}$, $\mathbf{H}_k \in \mathbf{R}^{r\times q}$, $\mathbf{R}_1$ and $\mathbf{H}_1$ are generated randomly, $\boldsymbol{\lambda}1_k \in \mathbf{R}^{m\times q}$, $\boldsymbol{\lambda}2_k \in \mathbf{R}^{r\times q}$; $\boldsymbol{\lambda}1_1$ and $\boldsymbol{\lambda}2_1$ are zero matrix. $\mathbf{L} = \mathbf{G}^{1/2}\mathbf{SW}_\mathrm{k} - \boldsymbol{\lambda}2_k/\rho$; $\mathbf{v}$ is the row vector of $\mathbf{W}_k - \boldsymbol{\lambda}1_k/\rho$.

Finally, we use the alternating direction multiplier method [45] to solve the variables in iterative equations (12) to receive the optimal weight $\mathbf{W}$ of the feature layer, and then the mapping feature $\mathbf{Z}$ could be obtained by bringing $\mathbf{W}$ into the mapped feature (1).

After extracting $\mathbf{Z}$ from the feature layer, supposing there are p enhancement nodes, and we could receive the enhancement information $\mathbf{H}$ by bringing $\mathbf{Z}$ into the enhanced information (2).

The augmented input $[\mathbf{Z}|\mathbf{H}]$ of the feature layer and the enhancement layer is obtained, and then the output of RMWAD model is $[\mathbf{Z}|\mathbf{H}]\mathbf{W}_{\text{out}}$, and then we could receive the relationship between the predicted value and the true value

$$s(t+1) \approx [\mathbf{Z}|\mathbf{H}]\mathbf{W}_{\text{out}}, \tag{13}$$

where $\mathbf{W}_{\text{out}}$ is obtained by ridge regression algorithm [35], $s(t+1)$ is real value of prediction value.

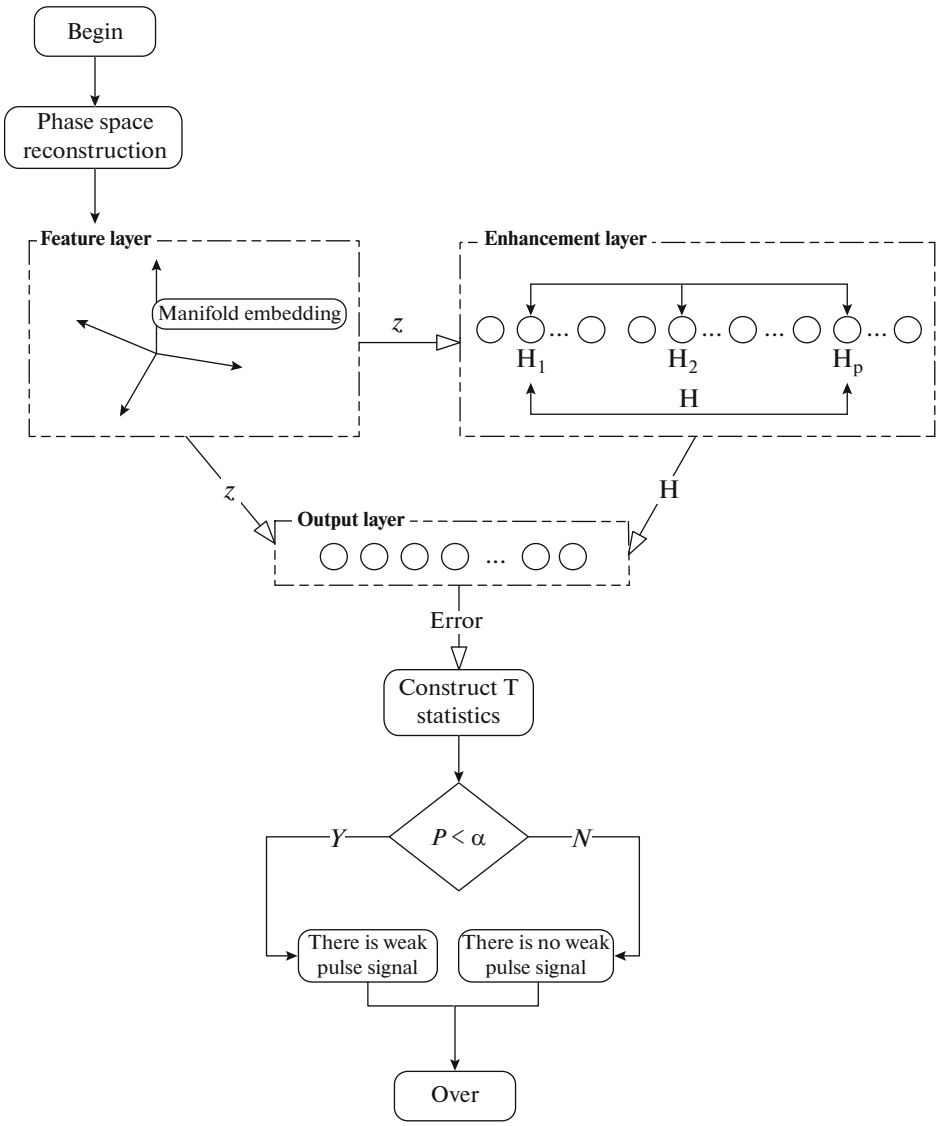

Fig. 2. The flow chart of the RMWAD model.

Then, we could establish the approximate mapping of reconstructed observation signal

$$s(t+1) \approx \hat{h}(\mathbf{S}(t)) \tag{14}$$

and we could receive the one-step prediction error by the relationship between the predicted value and the true value (13).

$$\hat{e}(t+1) = \hat{h}(\mathbf{S}(t)) - s(t+1). \tag{15}$$

Supposing $\hat{e}(n+1) \sim N(0, \sigma^2)$, n is the number of samples, and the hypothesis test is as the follows:

H_0: there is no u_t in the observed signal.

H_1: there is u_t in the observed signal,

where u_t represents the weak pulse signal. Then, we could establish T statistics

$$T = \frac{\hat{e}(n+1) - E(\hat{e}(n+1))}{S_{\hat{e}(n+1)}}, \tag{16}$$

if H_0 is true, then $T \sim t(n-1)$, and $\forall\, \alpha \in (0,1)$, we could receive $P = \{|T| \geq |t_0|\}$, where α is confidence coefficient, and

$$t_0 = \frac{\hat{e}(n+1) - E(\hat{e}(n+1))}{S_{\hat{e}(n+1)}}. \tag{17}$$

When $P < \alpha$, we could reject the original hypothesis and consider that there is a weak pulse signal in the observation signal, and the hypothesis threshold $t_{\alpha/2}(n-1)$ could be obtained from the t distribution

table. According to the dynamic threshold, we could realize adaptive detection to make the signal detection result more objective.

In summary, the flow chart of RMWAD model detecting weak pulse signal is shown in Fig. 2.

3. SIMULATION EXPERIMENTS

In this section, we perform three simulation experiments to verify the feasibility and effectiveness of the RMWAD model. In the experiment, we would use the chaotic background signals generated by the Lorenz system and Rosser system, the signal-to-noise ratio (SNR) is used to evaluate the detection threshold, the mean absolute error (MAE) and root mean square error (RMSE) are used to evaluate the prediction error of the model, and the ROC curve and its area under (AUC), accuracy rate (PR), recall rate (RE), accuracy rate (ACC) and F1 score (F1) are used as the evaluation index of detection results:

$$1)\ \mathrm{SNR} = 10\log\left(\frac{\sigma_u^2}{\sigma_n^2+\sigma_e^2}\right),$$

$$2)\ \mathrm{MAE} = \frac{1}{n}\sum_{i=1}^{n}\left|\hat{u}(t)-u(t)\right|,$$

$$3)\ \mathrm{RMSE} = \sqrt{\frac{1}{n}\sum_{i=1}^{n}(\hat{u}(t)-u(t))^2},$$

$$4)\ \mathrm{PR} = \frac{\mathrm{TP}}{\mathrm{TP}+\mathrm{FP}},$$

$$5)\ \mathrm{RE} = \frac{\mathrm{TP}}{\mathrm{TP}+\mathrm{FN}},$$

$$6)\ \mathrm{ACC} = \frac{\mathrm{TP}+\mathrm{TN}}{\mathrm{TP}+\mathrm{TN}+\mathrm{FP}+\mathrm{FN}},$$

$$7)\ \mathrm{F1} = \frac{2\mathrm{PR}\times\mathrm{RE}}{\mathrm{PR}+\mathrm{RE}}$$

where

$$\sigma_u^2 = \frac{1}{n}\sum_{i=1}^{n}\left(u(t)-\overline{u}(t)\right) \tag{18}$$

and

$$\sigma_n^2 = \frac{1}{n}\sum_{i=1}^{n}\left(n(t)-\overline{n}(t)\right), \tag{19}$$

σ_e^2 is the variance of white noise, σ_n^2 is the variance of chaotic signal, σ_u^2 is the the variance of weak pulse signal, $u(t)$ is wake pulse signal and $\hat{u}(t)$ is the prediction value of the RMWAD model to $u(t)$. TP refers to the number of times when there is a pulse signal in the observation signal and it is judged to have a pulse signal; TN refers to the number of times when there is no pulse signal and it is judged to have no pulse signal; FP refers to the number of times when there is no pulse signal but it is judged to have a pulse signal; FN refers to the number of times when there is a pulse signal but it is judged to have no pulse signal.

The iterative equation of the Lorenz system is as follows:

$$\mathrm{Lorenz} = \begin{cases}\dot{x} = \alpha(y-x),\\ \dot{y} = x(\gamma-z)-y,\\ \dot{z} = xy-\beta z.\end{cases} \tag{20}$$

The iterative equation of the Rosser system is as follows:

$$\mathrm{Rosser} = \begin{cases}\dot{x} = -(y+z),\\ \dot{y} = x+ay,\\ \dot{z} = b+z(x-c),\end{cases} \tag{21}$$

where x, y, z is the function of time. Supposing the initial condition $x(0)=1$, $y(0)=1$, $z(0)=1$, the sampling time is $t=0.01$ s, and we could generate 10000 data points by the fourth-order method, and the first component is taken as the chaotic background. In addition, in order to ensure the complete chaotic state of the system, we could abandon the previous 3000 points and select 4000 continuous sequences as the chaotic background denoted by $n(t)$.

The white noise uses the wgn function in Matlab to generate a one-dimensional sequence of 4000 samples that obey the normal distribution denoted by $e(t)$, and then, we could use the sum of $n(t)$ and $e(t)$ as the chaotic noise background, where the mean of the white noise is equal to zero, and the values of σ_e are shown in Tables 2 to 5 respectively.

The parameters used in the simulation experiments are shown in Table 1.

3.1. Experiment 1: Detecting the Existence of Weak Pulse Signal

Suppose that the pulse signal is a single pulse signal, that is

$$u(t) = a_1 u_1(t),$$
$$u(t) = \begin{cases}1, & t = \{400, 800, 1200, 2600, \ldots\},\\ 0, & \text{otherwise},\end{cases}$$

we generate a time series with length of 4000, denoted by $\{u(t), t = 1, 2, \ldots, 4000\}$, and detect weak pulse signals by using the RMWAD model.

For the Lorenz system, $a_1 = 2.5$, $\sigma_u = 0.1248$, $\sigma_n = 7.8640$, $\sigma_e = 0.0096$, SNR = −82.8589 dB, and then the detection results of are shown in Fig. 3. For the Rosser system, $a_1 = 0.4$, $\sigma_u = 0.0200$, $\sigma_n = 5.1025$, $\sigma_e = 8.7768\times10^{-4}$, SNR = −110.8599 dB, and then the detection results are shown in Fig. 4.

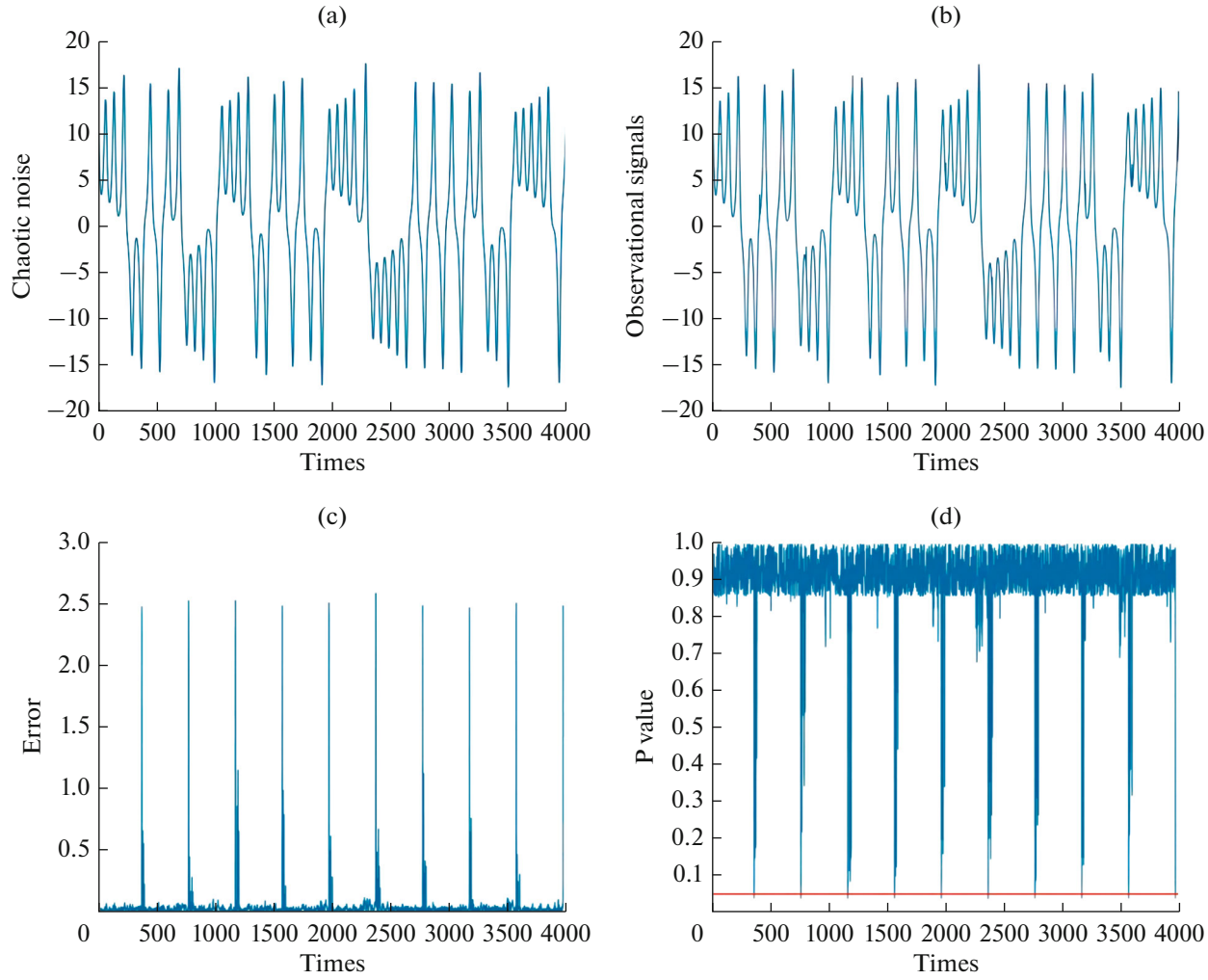

Fig. 3. Detection results of the RMWAD model: (a) Lorenz noise signal; (b) observation signal; (c) the one-step prediction error of observed signal with Lorenz; (d) P value.

Figures 3a, 3b respectively show the chaotic noise signal and observation signal of Lorenz system: according to Fig. 3b, the influence of weak pulse signal on chaotic noise background signal is very small, therefore, the embedding dimension and delay time of the chaotic noise background signal obtained by the same method are the same. Figures 3c, 3d are the one-step prediction error and dynamic threshold P value obtained by RMWAD model respectively: according to Fig. 3c, it shows that the error of 10 positions is obviously larger, and there may be a weak pulse signal. Combined with Fig. 3d, the P value of these 10 positions is less than 0.5, it shows that there are weak pulse signals in the observation signal under the Lorenz chaotic noise background based on subsection 1.2 hypothesis test.

The chaotic noise signal and observation signal of the Rosser system respectively are shown in Figs. 4a, 4b. The

Table 1. Experimental parameters

	Lorenz system	Rosser system	Phase space reconstruction	RMWAD model
Parameters value	$\alpha = 10,\ \beta = 8/3,\ \gamma = 28$	$a = 0.2,\ b = 0.2,\ c = 5.9$	$m = 6,\ \tau = 7$	$q = 6,\ p = 42$

τ is delay times, m is embedding dimension, q is number of feature nodes, p is the number of enhancement nodes.

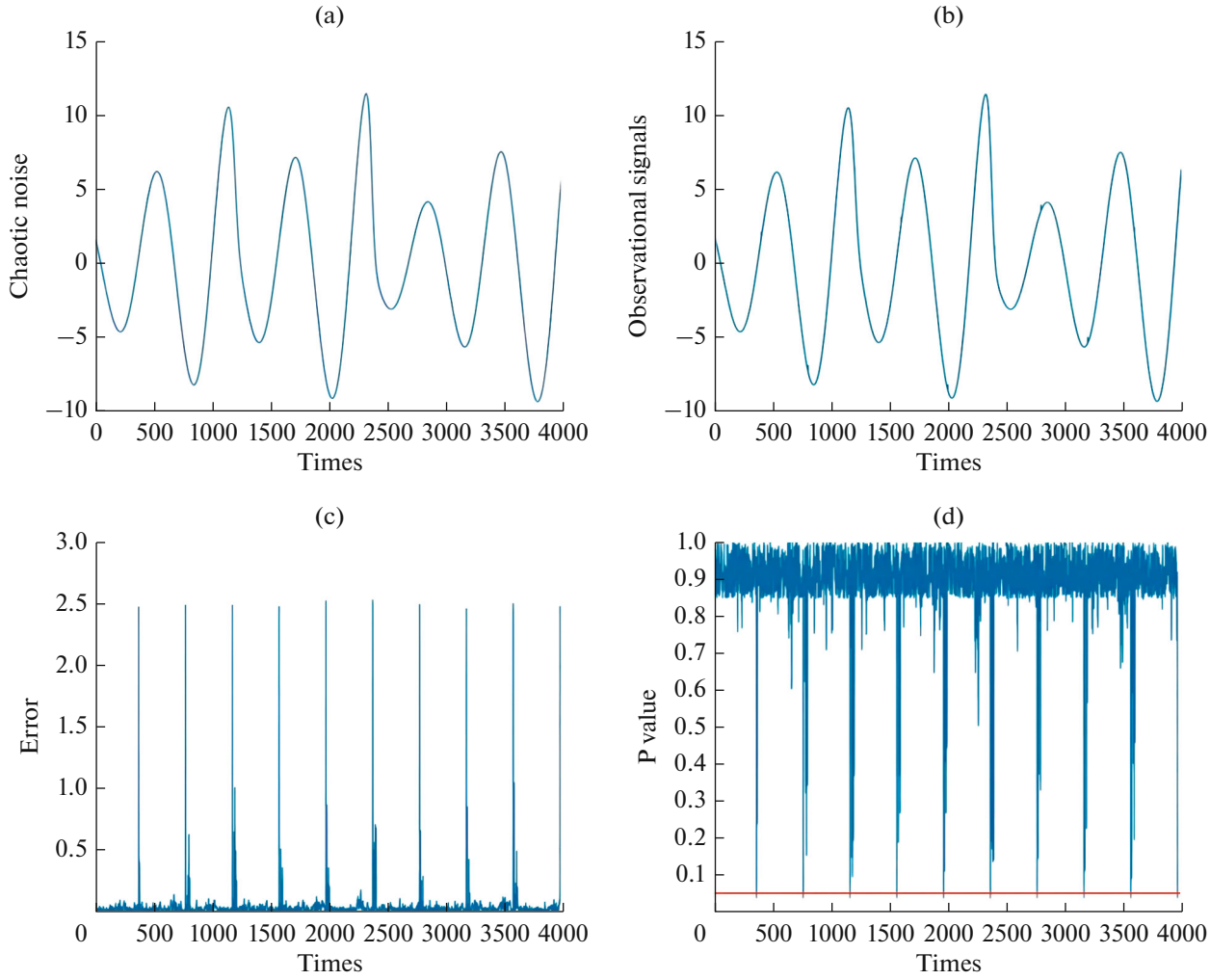

Fig. 4. Detection results of the RMWAD model under the Rosser noise background: (a) chaotic noise signal; (b) received signal; (c) the one-step prediction error; (d) P value.

one-step prediction error and dynamic threshold P value of RMWAD model respectively is shown in Figs. 4c, 4d: the 10 positions are relatively large and there may be weak pulse signal (see Fig. 4c), but it is not show that the weak pulse signal exist objectively. Therefore, the dynamic threshold obtained by the RMWAD model is further used to judge, the P value of hypothesis test is less than 0.5 (see Fig. 4d), and according to subsection 1.2 hypothesis test, it objectively shows that the observation signal under the Rosser chaotic noise background also exits weak pulse signal.

3.2. Experiment 2: Detection of Weak Pulse Signal under the Different SNR Condition

In the subsection, we would detect weak pulse signal under different SNR to receive the range of detection of *SNR* by the RMWAD model. Suppose that the pulse signal is a single pulse signal, that is

$$u(t) = a_1 u_1(t),$$
$$u(t) = \begin{cases} 1, & t = \{500, 1000, 1500, 2000, \ldots\}, \\ 0, & \text{otherwise}, \end{cases}$$

and we generate a time series with length of 4000, denoted by $\{u(t), t = 1, 2, \ldots, 4000\}$. We assume that the period of the weak pulse signal is constant, and the intensity of weak pulse signal is controlled by changing the value of a_1, the detailed values of a_1 and detection results are shown in Tables 2 and 3.

Table 2 shows that the detailed values of a_1 and detection results of the RMWAD model under the Lorenz chaotic noise background. It shows that with the decrease of the SNR, the value of MAE and RMSE become smaller and smaller (see Fig. 5a). According to Table 2, with the decrease of the SNR, the PR is always

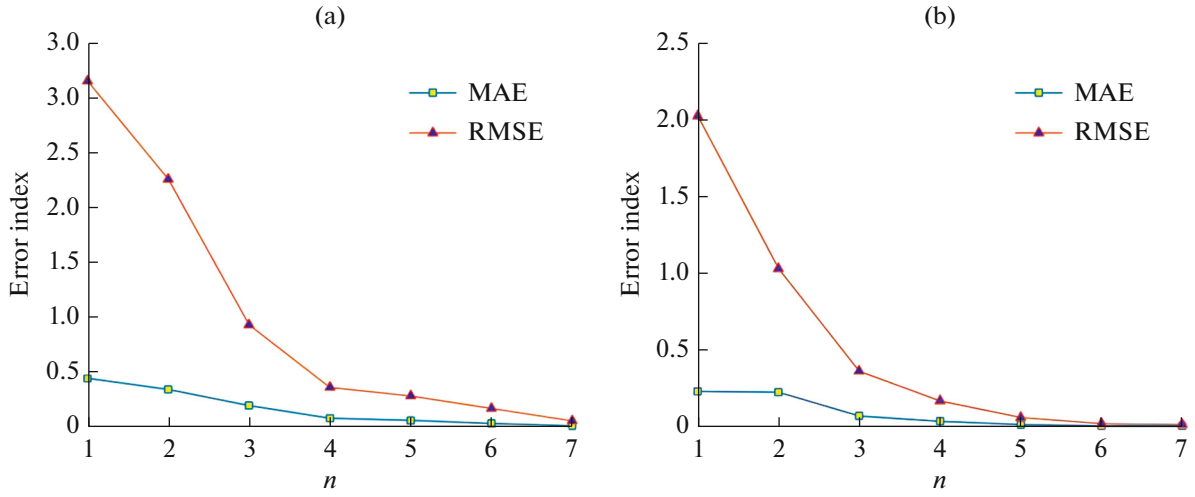

Fig. 5. The trend chart of error evaluation index under different SNR: (a) MAE and RMSE under the Lorenz noise background; (b) MAE and RMSE under the Rosser noise background.

equal to 1.0, and the ACC remains above 0.99. The RE decreases, but the lowest F1 for the comprehensive evaluation of PR and RE is 0.8, it shows that the RMWAD model could effectively detect the weak pulse signal in $\mathrm{SNR} \in (-103.4120\ \mathrm{dB}, -18.4453\ \mathrm{dB})$.

Table 3 shows that the detailed values of a_1 and detection results of the RMWAD model under the Rosser noise chaotic background. It also shows that the value of MAE and RMSE of the model are getting smaller and smaller with the decrease of the SNR (see Fig. 5b). According to Table 3, the value of PR is always 1.0, the value of ACC remains above 0.99, and the value of F1 is also not less than 0.8, it shows that the model could also detect weak pulse signal well in $\mathrm{SNR} \in (-126.9493\ \mathrm{dB}, -16.5239\ \mathrm{dB})$.

3.3. Experiment 3: Comparison of Different Models for Weak Pulse Signal Detection

In the subsection, we compare the RMWAD model with extreme gradient boosting (XGB) model, back propagation (BP) neural network model, broad learning system (BLS) model and support vector regression (SVR) model. It is assumed that the pulse signal is the same single pulse signal as the experiment 2, we use above different models to detect the weak pulse signal under the chaotic noise background of the Lorenz system and Rosser system respectively, use MAE, RMSE to evaluate the prediction error of the model, and use ROC curve, PR, RE, ACC, F1 to evaluate the detection performance.

Table 2. Detection results for the Lorenz system

SNR	White noise	Evaluation index of prediction error		Detection performance evaluation index			
dB	σ_e	MAE	RMSE	PR	RE	ACC	F1
−18.4453(70)	0.2404	0.4500	3.1714	1.0	1.0	1.0	1.0
−25.1732(50)	0.1759	0.3474	2.2724	1.0	1.0	1.0	1.0
−43.4976(20)	0.0698	0.1999	0.9393	1.0	1.0	1.0	1.0
−65.9760(6.5)	0.0277	0.0840	0.3664	1.0	0.7272	0.9992	0.8421
−71.2233(5)	0.0175	0.0646	0.2878	1.0	0.6667	0.9989	0.8000
−81.4398(3)	0.0105	0.0361	0.1738	1.0	0.6667	0.9989	0.8000
−103.4120(1)	0.0035	0.0142	0.0598	1.0	0.6667	0.9989	0.8000

The value of a_1 is in brackets.

Table 3. Detection results for the Rosser system

SNR	White noise	Evaluation index of prediction error		Detection performance evaluation index			
dB	σ_e	MAE	RMSE	PR	RE	ACC	F1
−16.5239(50)	0.0994	0.2280	2.0234	1.0	1.0	1.0	1.0
−34.8465(20)	0.0403	0.2227	1.0283	1.0	1.0	1.0	1.0
−57.3246(6.5)	0.0128	0.0675	0.3595	1.0	1.0	1.0	1.0
−72.7883(3)	0.0060	0.0328	0.1660	1.0	1.0	1.0	1.0
−94.7616(1)	0.0020	0.0114	0.0581	1.0	1.0	1.0	1.0
−118.8400(0.3)	6.1183×10^{-4}	0.0035	0.0178	1.0	0.8	0.9995	0.8889
−126.9493(0.2)	3.9968×10^{-4}	0.0021	0.0118	1.0	0.7272	0.9992	0.8421

The value of a_1 is in brackets.

Table 4. Comparison of different models under different SNR for the Lorenz system

		RMWAD	XGB	BP	BLS	SVR
SNR	dB	−103.4120	−81.4398	−71.2233	−65.9760	−43.4976
White noise	σ_e	0.0035	0.0105	0.0175	0.0277	0.0698
Evaluation index of prediction error	MAE	0.0142	0.0331 (0.0361)	0.0891 (0.0646)	0.1184 (0.0840)	1.9688 (0.1999)
	RMSE	0.0598	0.0472 (0.1738)	0.3454 (0.2878)	0.4267 (0.3664)	2.5146 (0.9393)
Detection performance evaluation index	ACC	0.9989	0.9982 (0.9989)	0.9984 (0.9989)	0.9985 (0.9992)	0.9990 (1.0)
	PR	1.0	0.25 (1.0)	1.0 (1.0)	1.0 (1.0)	0.5 (1.0)
	RE	0.6667	0.6667 (0.6667)	0.5714 (1.0)	0.5714 (1.0)	1.0 (1.0)
	F1	0.8000	0.3636 (0.8000)	0.7272 (0.8000)	0.7272 (0.8421)	0.6667 (1.0)

The value of the RMWAD model in the same SNR in brackets.

The detection results of models under the Lorenz system and Rosser system chaotic background are shown in Tables 4 and 5 respectively.

In the Table 4, SNR = −103.4120 dB, the PR and ACC values of the RMWAD model are above 0.99, and the value of F1 of the comprehensive evaluation of PR and RE is 0.8, AUC (see Fig. 6a) value is over than other models. In addition, the SNR of other models are higher than that of the RMWAD model, but their detection performance is not as good as the RMWAD model.

In the Table 5, SNR = −126.9493 dB, the prediction error of the RMWAD model is relatively small than other models, and the ACC and PR values are also above 0.99. The evaluation detection index values of other models are not as good as the RMWAD model. In addition, the AUC values of other models are smaller than the RMWAD model (see Fig. 6b), Therefore, it shows that the RMWAD model has better detection performance than other models under the Rosser chaotic noise background.

CONCLUSIONS

We have established a new RMWAD model to detect weak pulse signal under the chaotic noise background. Considering the short-term predictability and sensitivity to small disturbance of chaotic time series,

Table 5. Comparison of different models under different SNR for the Rosser system

		RMWAD	XGB	BP	BLS	SVR
SNR	dB	−126.9493	−118.8400	−94.7616	−86.6513	−57.3246
White noise	σ_e	3.9968×10^{-4}	6.1183×10^{-4}	0.0020	0.0029	0.0128
Evaluation index of prediction error	MAE	0.0021	0.0162 (0.0035)	0.0160 (0.0114)	0.0178 (0.0173)	5.7582 (0.0675)
	RMSE	0.0118	0.0225 (0.0178)	0.0597 (0.0581)	0.0881 (0.0850)	7.1170 (0.3595)
Detection performance evaluation index	ACC	0.9992	0.9982 (0.9995)	0.9985 (1.0)	0.9984 (1.0)	0.9980 (1.0)
	PR	1.0	0.25 (1.0)	1.0 (1.0)	1.0 (1.0)	0.0 (1.0)
	RE	0.7272	0.6667 (0.8)	0.5714 (1.0)	0.5714 (1.0)	NAN (1.0)
	F1	0.8421	0.3636 (0.8889)	0.7272 (1.0)	0.7272 (1.0)	NAN (1.0)

The value of the RMWAD model in the same SNR in brackets.

we construct the RMWAD model combined with phase space reconstruction. We detect weak pulse signal under Lorenz and Rosser chaotic noise background respectively by using the RMWAD model. The Results of the simulation experiments are as follows:

(1) According to experiment 1, there is a wake pulse signal in the observation signal, and the RMWAD model could detect weak pulse signal from the Lorenz and Rosser chaotic noise background respectively.

(2) According to experiment 2, for Lorenz chaotic noise background, it shows that the RMWAD model could effectively detect weak pulse signal in SNR $\in (-103.4120\text{ dB}, -18.4453\text{ dB})$, and the value of AUC, PR, ACC and F1 are relatively high; for the Rosser noise chaotic background, the RMWAD model could also detect weak pulse signal in SNR $\in (-126.9493\text{ dB}, -16.5239\text{ dB})$, and the values of AUC, PR, ACC and F1 are relatively high.

(3) According to experiment 3, the RMWAD model has better detection performance for weak pulse signals under chaotic noise background than BLS, BP, XGBOOST and SVR models under the same SNR or

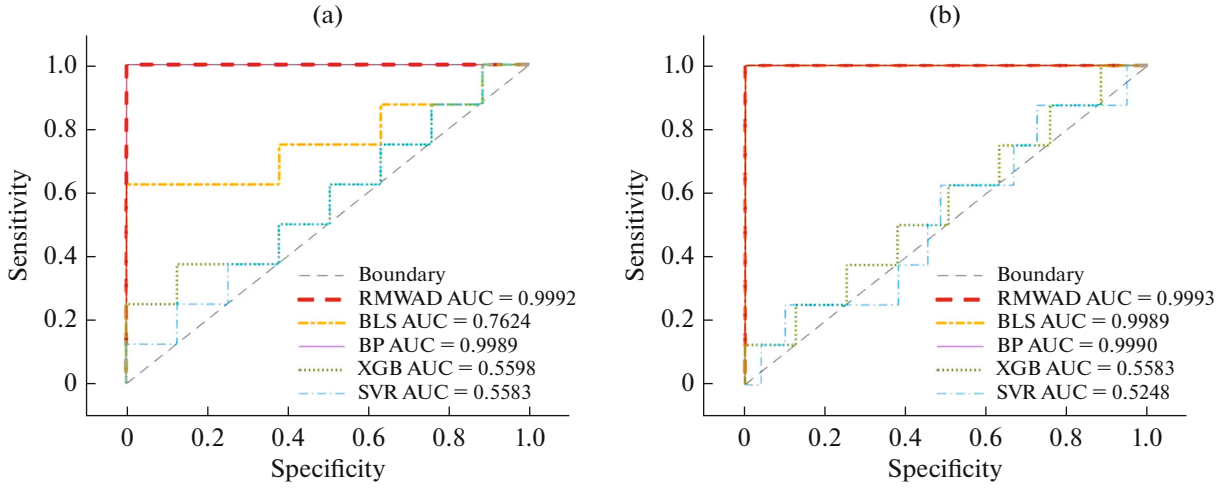

Fig. 6. ROC curves of different models in the same SNR: (a) SNR = −103.4120 dB in the Lorenz noise background; (b) SNR = −126.9493 dB in the Rosser noise background.

different SNR, and the prediction error of this model is relatively small.

In summary, the RMWAD model proposed by this paper is effective and simple for weak pulse signal detection under the chaotic noise background without additional prior knowledge. In the future, we will continue to improve the prediction error and detection performance of the RMWAD model to achieve lower SNR operating threshold and extend it to the detection of other signals.

FUNDING

This work was supported by the Natural Science Foundation of China, grant no. 11871124 and Chongqing Natural Science Foundation of China, grant no. cstc2018jcyjAX0464).

DATA AVAILABILITY

No data were used to support this study.

CONFLICTS OF INTEREST

The authors declare that they have no conflicts of interest.

REFERENCES

1. K. M. Hock, "Narrowband weak signal detection by higher order spectrum," IEEE Trans. Signal Process. **44**, 874–879(1996). https://doi.org/10.1109/78.492540
2. H. Xing, Q. Zhu, and W. Xu, "A weak signal detection method under chaotic sea clutter background," Acta Phys. Sinica **63** (10), 45–51 (2014). https://doi.org/10.7498/aps.63.100505
3. M. Kalra, S. Kumar, and B. Das, "Seismic signal analysis using empirical wavelet transform for moving ground target detection and classification," IEEE Sensors J. **20** (14), 7886–7895(2020). https://doi.org/10.1109/JSEN.2020.2980857
4. S. Kikuchi, H. Takeuchi, O. Mori, H. Kato, and S. Taniguchi, "Off-line signal processing for weak-signal detection and orbit and attitude determination," J. Spacecraft & Rockets **56**, 1–12 (2018). https://doi.org/10.2514/1.A34201
5. J. J. Collins, C. C. Chow, and T. T. Imhoff., "Stochastic resonance without tuning," Nature **376** (6537), 236–238 (1995). https://doi.org/10.1038/376236a0
6. Q. He and J. Wang, "Effects of multiscale noise tuning on stochastic resonance for weak signal detection," Digital Signal Process. **22**, 614–621, (2012). https://doi.org/10.1016/j.dsp.2012.02.008
7. Scofield, H. John, "Frequency-domain description of a lock-in amplifier," Am. J. Phys. **62**, 129–133(1994). https://doi.org/10.1119/1.17629
8. A. D. Marcellis, "A fully-analog lock-in amplifier with automatic phase alignment for accurate measurements of ppb gas concentrations," IEEE Sensors J. **12**, 1377–1383 (2012). https://doi.org/10.1109/JSEN.2011.2172602
9. G. Wang and D. Chen, "The application of chaotic oscillators to weak signal detection," IEEE Trans. Industrial Electronics, **46**, 440–444 (1999). https://doi.org/10.1109/41.753783
10. H. Vahedi, G. B. Gharehpetian, and M. Karrari, "Application of duffing oscillators for passive islanding detection of inverter-based distributed generation units," IEEE Trans. Power Delivery **27**, 1973–1983 (2012). https://doi.org/10.1109/TPWRD.2012.2212251
11. S. Haykin and B. L. Xia, "Detection of signals in chaos," Proc. IEEE **83**, 95–122 (1995). https://doi.org/10.1109/5.362751
12. L. Su, H. sun, J. Wang, and L. Yang, "Detection and recovery of weak pulse signal under chaotic noise background," Acta Physica Sinica **66** (9), 29–38, (2017). https://doi.org/10.7498/aps.66.090503
13. M. Fedula, T. Hovorushchenko, A. Nicheporuk, and V. Martynyuk, "Chaos-based signal detection with discrete-time processing of the Duffing attractor," Eastern-Eur. J. Enterprise Technol. **4** (100), 44–51 (2019). https://doi.org/10.15587/1729-4061.2019.175787
14. C. Li and L. Su, "Extracting harmonic signal from a chaotic background with local linear model," Mech. Syst. & Signal Process. **84** (1), 499–515 (2017). https://doi.org/10.1016/j.ymssp.2016.07.040
15. Q. Li, X. Xu and L. Yin, "Implication of two-coupled tristable stochastic resonance in weak signal detection," Chinese Phys. B **27**, 260–266 (2018). https://doi.org/10.1088/1674-1056/27/3/034203
16. P. H. Jau, Z. M. Tsai, N. C. Kuo, J. C. Kao, K. Y. Lin, F. R. Chang, E. C. Yang, and H. Wang, "Signal processing for harmonic pulse radar based on spread spectrum technology," IET Radar, Sonar and Navigation **8** (3), 242–50 (2014). https://doi.org/10.1049/iet-rsn.2013.0024
17. L. Su, L. Deng, W. Zhu, and S. Zhao, "Statistical detection of weak pulse signal under chaotic noise based on Elman neural network," Wireless Commun. Mobile Comput. **2020**, 1–12 (2020). https://doi.org/10.1155/2020/9653586
18. S. Haykin and H. Leung, "Chaotic model of sea clutter using a neural network," Proc. SPIE **1152**, 18–21 (1989). https://doi.org/10.1117/12.962261
19. R. Paffenroth, P. du Toit, R. Nong, L. Scharf, A. P. Jayasumana, and V. Bandara, "Space-time signal processing for distributed pattern detection in sensor networks," IEEE J. Select. Top. Signal Process. **7** (1), 38–49 (2013). https://doi.org/10.1109/JSTSP.2012.2237381
20. J. Suykens and J. Vandewalle, "Least Squares Support Vector Machine Classifiers," Neural Process. Lett. **9**, 293–300 (1999). https://doi.org/10.1023/A:1018628609742
21. H. Xing, Y. Cheng, and W. Xu, "Weak signal detection in chaotic background based on generalized window function and least squares support vector machine," Acta Phys. Sinica **61** (10), 59–68 (2012). https://doi.org/10.7498/aps.61.100506
22. J. Park, G. Shevlyakov, and K. Kim, "Distributed detection and fusion of weak signals in fading channels with non-Gaussian noises," IEEE Commun. Lett. **16**,

220–223 (2012).
https://doi.org/10.1109/LCOMM.2011.121311.111870

23. L. Su and C. Li, "Extracting narrow-band signal from a chaotic background with LLVCR," Wireless Personal Commun. **96**, 1907–1927 (2017).
https://doi.org/10.1007/s11277-017-4275-3
24. C. L. Chen and Z. Liu, "Broad learning system: an effective and efficient incremental learning system without the need for deep architecture," IEEE Trans. Neural Netw. Learn. Syst. **29** (99), 10–24 (2018).
https://doi.org/10.1109/TNNLS.2017.2716952
25. M. Han, S. Feng, C. L. Chen, M. Xu, and T. Qiu, "Structured manifold broad learning system: A manifold perspective for large-scale chaotic time series analysis and prediction," IEEE Trans. Knowledge & Data Eng. **31**, 1809–1821 (2018).
https://doi.org/10.1109/TKDE.2018.2866149
26. S. Feng, W. Ren, M. Han, and Y. W. Chen, "Robust manifold broad earning system for large-scale noisy chaotic time series prediction: A perturbation perspective," Neural Networks **117** (5), 179–190 (2019).
https://doi.org/10.1016/j.neunet.2019.05.009
27. H. Zhao, J. Zheng, J. Xu, and W. Deng, "Fault diagnosis method based on principal component analysis and broad learning system," IEEE Access **7**, 99263–99272 (2019).
https://doi.org/10.1109/ACCESS.2019.2929094
28. J. Fan, X. Wang, X. Wang, J. Zhao, and X. Liu, "Incremental wishart broad learning system for fast PolSAR image classification," IEEE Geosci. & Remote Sensing Lett. **16**, 1854–1858 (2019).
https://doi.org/10.1109/LGRS.2019.2913999
29. S. Issa, Q. Peng, and X. You, "Emotion classification using EEG brain signals and the broad learning system," in IEEE Trans. Syst., Man, and Cybern.: Systems. 1–10 (2020).
https://doi.org/10.1109/TSMC.2020.2969686
30. L. Xu, C. L. P. Chen, and R. Han," Sparse Bayesian broad learning system for probabilistic estimation of prediction," IEEE Access **8**, 56267–56280 (2020).
https://doi.org/10.1109/ACCESS.2020.2982214
31. Z. Shi, X. Chen, C. Zhao, H. He, V. Stuphorn, and D. Wu, "Multi-view broad learning system for primate oculomotor decision decoding," IEEE Trans. Neural Syst. Rehabilitat. Eng. **28**, 1908–1920 (2020).
https://doi.org/10.1109/TNSRE.2020.3003342
32. C. Ren, Y. Chao, Y. Sun, Z. Liu, and J. Chen, "Research progress of broad learning system," Computer Appl. Res. **38**, 2258–2267 (2021).
https://doi.org/10.19734/j.issn.1001-3695.2020.11.0348
33. M. Adegoke, H. T. Wong, and C. S. Leung, "A fault aware broad learning system for concurrent network failure situations," IEEE Access **9**, 46129–46142 (2021).
https://doi.org/10.1109/ACCESS.2021.3066217
34. Y.-H. Pao, G.-H. Park, and D. J. Sobajic, "Learning and generalization characteristics of the random vector functional-link net," Neurocomputing **6** (2), 163–180 (1994).
https://doi.org/10.1016/0925-2312(94)90053-1
35. S. Freek and S. Olivier, "Many regression algorithms, one unified model: A review," Neural Networks: The Official J. Int. Neural Network Soc. **69**, 60–79 (2015).
https://doi.org/10.1016/j.neunet.2015.05.005
36. S. Feng and C. L. Chen, "Fuzzy broad learning system: A novel neuro-fuzzy model for regression and classification," IEEE Trans. Cybern. **1** (99), 1–11 (2018).
https://doi.org/10.1109/TCYB.2018.2857815
37. F. Takens, "Detecting strange attractors in turbulence," Lecture Notes in Math., **898** (1), 336–381(1980).
https://doi.org/10.1007/BFb0091924
38. L. Su, L. Deng, W. Zhu, and S. Zhao, "Detection and extraction of weak pulse signals in chaotic noise with PTAR and DLTAR models," Math. Problems in Eng. **2019**, 1–12 (2019).
https://doi.org/10.1155/2019/4842102
39. L. Cao, "Practical method for determining the minimum embedding dimension of a scalar time series," Physica. D: Nonlin. Phenom. **110** (1), 43–50 (1997).
https://doi.org/10.1016/S0167-2789(97)00118-8
40. A. M. Albano, J. Muench, C. Schwartz, A. I. Mees, and P. E. Rapp, "Singular-value decomposition and the Grassberger–Procaccia algorithm," Phys. Rev. A **38**, 3017–3026 (1988).
https://doi.org/10.1103/PhysRevA.38.3017
41. J. Gui., Z. Sun., S. W. Ji, D. C. Tao, and T. N. Tan, "Feature selection based on structured sparsity: A comprehensive study," IEEE Trans. Neural Networks and Learn. Syst. **28**, 1490–1507(2016).
https://doi.org/10.1109/TNNLS.2016.2551724
42. R. Lai and S. Osher, "A splitting method for orthogonality constrained problems," J. Sci. Comput. **58**, 431–449 (2014).
https://doi.org/10.1007/s10915-013-9740-x
43. Z. Wen and W. Yin, "A feasible method for optimization with orthogonality constraints," Math. Program. **142**, 397–434 (2013).
https://doi.org/10.1007/s10107-012-0584-1
44. J. Huang, F. Nie, H. Huang, and C. Ding, "Robust manifold non negative matrix factorization," ACM Trans. Knowl. Discov. from Data **8**, 121–125 (2014).
https://doi.org/10.1145/2630992
45. S. Boyd, N. Parikh, E. Chu, B. Peleato, and J. Eckstein, "Distributed optimization and statistical learning via the alternating direction method of multipliers," Foundat. & Trends Mach. Learn. **3** (1), 1–122 (2011).
https://doi.org/10.1561/2200000016